



Heat capacity, entropy, dielectric properties and T–p phase diagram of $(\text{NH}_4)_3\text{TiF}_7$



E.I. Pogoreltsev^{a,b,*}, I.N. Flerov^{a,b}, A.V. Kartashev^a, E.V. Bogdanov^{a,c}, N.M. Laptash^d

^a L.V. Kirensky Institute of Physics, Siberian Department of RAS, 660036 Krasnoyarsk, Russia

^b Siberian Federal University, 660074 Krasnoyarsk, Russia

^c Krasnoyarsk State Agrarian University, 660049 Krasnoyarsk, Russia

^d Institute of Chemistry, Far Eastern Department of RAS, 690022 Vladivostok, Russia

ARTICLE INFO

Article history:

Received 15 July 2014

Received in revised form 20 October 2014

Accepted 22 October 2014

Available online 31 October 2014

Keywords:

Cubic fluorides

Phase transitions

Dielectric

Phase diagram

Calorimetry

ABSTRACT

Successive phase transitions $G1 \rightarrow G2 \rightarrow G3$ in the double salt $(\text{NH}_4)_3\text{TiF}_7$ have been studied by detailed calorimetric, DTA under hydrostatic pressure and dielectric measurements. Rather large entropy jumps at phase transition points were found to be followed by large additional contributions associated with the temperature dependence of the excess heat capacity. The permittivity behaviour and the tangent of the dielectric losses proved the nonferroelectric nature of both transformations. Two triple-points were found on the temperature–pressure phase diagram, suggesting the existence of a hypothetical parent $G0 \equiv Pm\bar{3}m$ cubic phase. A direct transformation between high ($G0$) and low ($G3$) temperature cubic phases takes place at $p > 0.41$ GPa with a baric coefficient $dT_{G0 \rightarrow G3}/dp = -40$ K/GPa.

© 2014 Elsevier B.V. All rights reserved.

1. Introduction

Many fluorides containing anionic entities with six or seven ions in coordination may be combined to form many series of compounds with different crystal lattice symmetries. The best known examples among them are perovskites AMeF_3 , layered perovskites AMeF_4 and A_2MeF_4 , elpasolites $\text{A}_2\text{A}'\text{MeF}_6$, cryolites A_3MeF_6 , antiferrofluorites A_2MeF_6 , etc. [1–3]. Many of the crystals belonging to these families undergo phase transitions upon cooling and heating and show very rich phase sequences in T–p phase diagrams. Compared to these fluorides, the physical properties of compounds containing seven fluorine atoms in their general chemical formulation have been studied to a significantly less degree.

Double fluoride salts $\text{A}_3\text{MeF}_7 = \text{A}_2\text{MeF}_6 \cdot \text{AF}$ have been known for more than 70 years and are characterized by different room temperature symmetries of the crystal lattice depending on the size of the central atom [4–9]. Such a situation could be considered as strong evidence for the possible existence of phase transitions in these compounds with temperature and/or pressure variations.

Recently such a supposition was confirmed by optical and differential scanning calorimetric (DSC) investigations of the stability of the room temperature $P4/mnc$ phase in a $(\text{NH}_4)_3\text{TiF}_7$ crystal [10]. An unusual succession of two structural phase transitions was observed upon heating and cooling (cubic– $G3$) ($T_{21} = 291$ K) \leftrightarrow (tetragonal1– $G2$) ($T_{11} = 360$ K) \leftrightarrow (tetragonal2– $G1$). It was found that both transformations were of the first order and were followed by rather large entropy changes. Moreover, the phase transition at T_2 was accompanied by the reversible cracking of crystals observed in polarizing-optic measurements, which allowed it to be considered a reconstructive transformation.

Because optical investigations showed rather pronounced temperature dependence of birefringence, it was worthwhile to perform more careful studies of heat capacity compared to DSC measurements [10] in order to obtain precise information on the total heat capacity as well as excess enthalpy and entropy associated with these phase transitions. In accordance with the important role of the size of the central atom in the formation of structural symmetry in double salts such as $\text{A}_2\text{MeF}_6 \cdot \text{AF}$ [4–9], it was possible to suppose a great effect of hydrostatic pressure on the stability of crystal phases in $(\text{NH}_4)_3\text{TiF}_7$.

The present paper is devoted to detailed studies of the thermal properties of $(\text{NH}_4)_3\text{TiF}_7$ crystals using an adiabatic calorimeter of high resolution and differential thermal analysis (DTA) using a

* Corresponding author at: Kirensky Institute of Physics, Akademgorodok 50, bld. 38, Krasnoyarsk 660036, Russia. Tel.: +7 391 249 45 07; fax: +7 391 2430 89 23. E-mail address: pepel@iph.krasn.ru (E.I. Pogoreltsev).

highly sensitive Ge–Cu thermocouple over wide ranges of temperature and pressure. All experiments were carried out on samples prepared from crystals grown and given a preliminary examination in [10]. To reach final conclusion about the absence of noncentrosymmetrical phases in titanate, the permittivity and tangent of the dielectric losses were also studied. The information obtained about enthalpy, entropy, and susceptibility to hydrostatic pressure of the phase transitions as well as the nature of the structural distortions is discussed.

2. Experimental results and discussion

The heat capacity measurements on $(\text{NH}_4)_3\text{TiF}_7$ were carried out by means of a homemade automated adiabatic calorimeter with three screens in order to minimize thermal losses [11]. The inaccuracy in the heat capacity determination did not exceed (0.2–0.4) % over the whole temperature range investigated (80–380 K). Calorimetric measurements were performed on the “quasi-ceramic” sample in the form of a pressed pellet 8 mm in diameter and 2 mm in height, prepared without heat treatment because of the presence of ammonium ions. The mass of the sample was 0.1253 g. Discrete as well as continuous heating was used to measure the heat capacity of the “sample + heater + contact grease” system. In the former case, the calorimetric step was varied from 1.5 to 3.0 K. In the latter case, the system was heated at rates $dT/dt \approx 0.15\text{--}0.30$ K/min. The heat capacity temperature dependence of the heater and contact grease were determined in individual experiments.

The measured temperature dependence of the molar heat capacity $C_p(T)$ of $(\text{NH}_4)_3\text{TiF}_7$ is shown in Fig. 1a. In accordance with the succession of two phase transitions $G1 \rightarrow G2 \rightarrow G3$ found in optic and DSC measurements [10], two $C_p(T)$ anomalies were observed with maximum values at $T_1 = 357.8 \pm 0.5$ K and $T_2 = 291.6 \pm 0.5$ K.

The temperature range near T_2 was studied using the quasistatic thermogram method upon heating at a rate of $dT/dt = 8 \times 10^{-3}$ K/min. It can be seen from Fig. 1b that the structural transformation is accompanied by absorption of latent heat, as follows from the very small values of the derivative $dT/dt \leq 10^{-3}$ K/min observed at the phase transition point over a certain period of time. Such a behaviour of temperature against time near T_2 points to the “spread” absorption of heat, which agrees well with the “smeared” restoration of birefringence upon heating from the G3 phase to G2 [10]. Both experimental facts point out to a reconstructive transformation.

In order to get information on the anomalous values of heat capacity ΔC_p , enthalpy ΔH and entropy ΔS , the lattice heat capacity C_{lat} was estimated by an approximation of the total $C_p(T)$ using combination of Debye’s and Einstein’s functions $C_{\text{lat}}(T) = A_1 D(\Theta_D/T) + A_2 E(\Theta_E/T)$. The experimental data far from the phase transition regions, at $T > 360$ K and $T < 200$ K, were taken in consideration. The characteristic Debye’s and Einstein’s temperatures were estimated as follows: $\Theta_D = 212.75$ K, $\Theta_E = 537.59$ K. The lattice contribution is shown as a dashed line in Fig. 1a. The average deviation of the experimental data from the smoothed curve $C_{\text{lat}}(T)$ does not exceed 0.75%.

Fig. 1c shows that a large excess heat capacity contribution to total $C_p(T)$ exists in the whole temperature range between T_1 and T_2 , which is in agreement with the strong temperature dependent behaviour of birefringence in phase G2 [10]. This anomalous heat capacity was also found over a wide temperature range below T_2 where birefringence is absent because of the optical isotropy of cubic phase G3 [10]. At both phase transitions the ΔC_p value is rather significant, about 18% compared to C_{lat} . Such a $\Delta C_p(T)$ behaviour means that the changes in the order parameters associated with the structural distortions in $(\text{NH}_4)_3\text{TiF}_7$ take place in the temperature region between 360 and 200 K.

The enthalpy of the phase transitions was determined by integration of the $\Delta H_i = \int \Delta C_p dT$ function. Transformation $G2 \rightarrow G3$ takes place when the process of structural distortions associated with the phase transition at T_1 is not completed ($\Delta C_p)_{T_1} \neq 0$ (Fig. 1c); but, because of a narrow temperature range below T_2 , where $(\Delta C_p)_{T_1}$ still exists, and huge values of ΔC_p at T_1 and T_2 , the uncertainty of the ΔH_i determination is rather small: $\Delta H_1 = 3400 \pm 200$ J/mol; $\Delta H_2 = 6700 \pm 400$ J/mol.

The temperature dependence of the excess entropy was determined by integration of the function $\Delta S = \int (\Delta C_p/T) dT$ (Fig. 2). First of all it is necessary to note that the sum of entropies associated with both phase transitions is rather large: $\sum \Delta S_i = \Delta S_1 + \Delta S_2 = 32 \pm 2$ J/mol K. Such a huge value of $\sum \Delta S_i$ is rare for phase transitions in ionic crystals and is usually associated with strong disorder in some structural units in the high temperature initial phase. The $\sum \Delta S_i$ value found in $(\text{NH}_4)_3\text{TiF}_7$ is comparable with entropy changes in oxyfluorides $(\text{NH}_4)_2\text{NbOF}_5$ ($\sum \Delta S_i \approx 37$ J/mol K) and $(\text{NH}_4)_3\text{NbOF}_6$ ($\sum \Delta S_i \approx 41$ J/mol K) resulting from two and four structural transformations, respectively, accompanied by the ordering of octahedral and tetrahedral ionic groups [12,13].

Individual values of entropy change in $(\text{NH}_4)_3\text{TiF}_7$ differ from each other significantly: $\Delta S_1 = 9.2 \pm 0.6$ J/(mol K) ($\sim R \ln 3$),

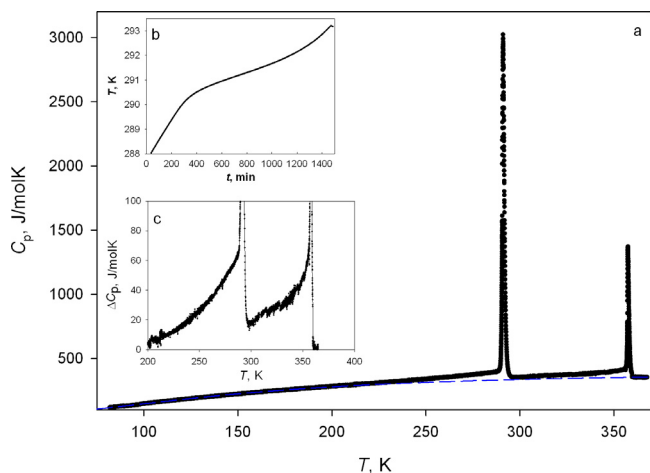


Fig. 1. Temperature dependence of the molar heat capacity of $(\text{NH}_4)_3\text{TiF}_7$. Dashed line is the lattice heat capacity (a). The results of a quasistatic thermogram study near the $G2 \rightarrow G3$ phase transition point (b). The excess heat capacity behaviour (c).

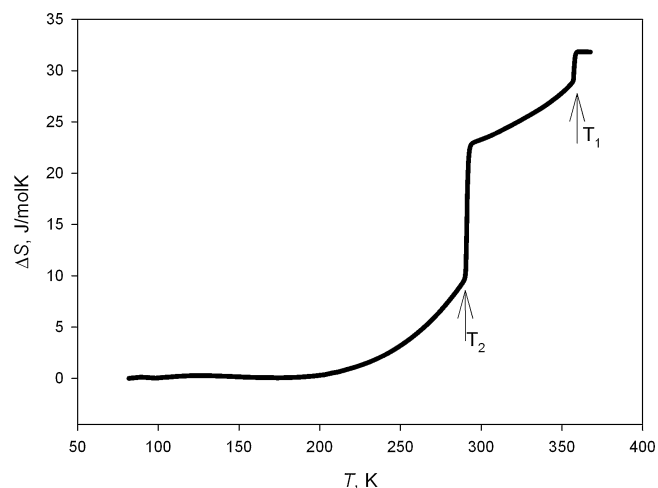


Fig. 2. Temperature dependence of the excess entropy associated with $G1 \rightarrow G2 \rightarrow G3$ phase transitions.

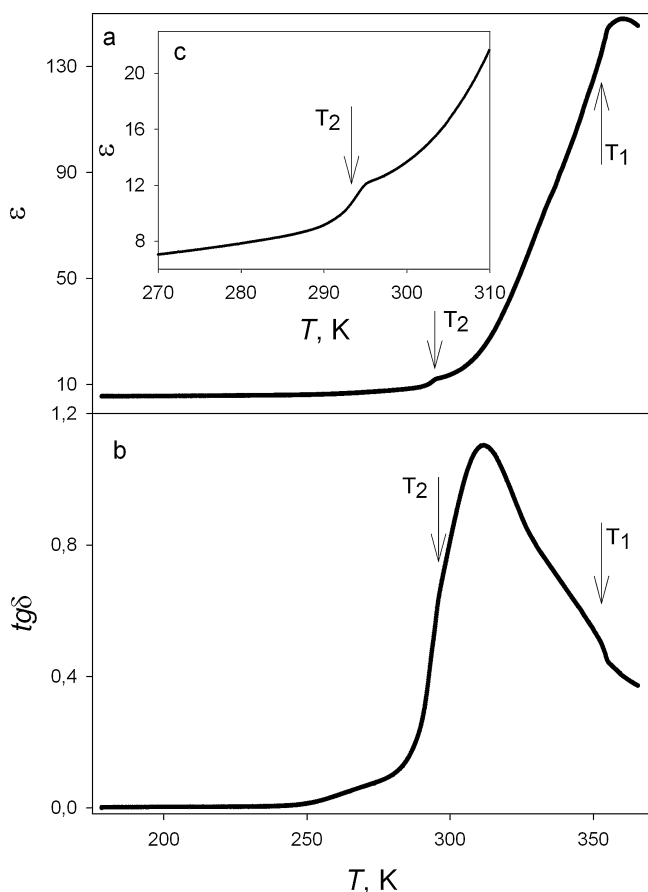


Fig. 3. Temperature dependencies of the permittivity ε over a wide temperature range (a) and in the region of T_2 (c), and the dielectric loss tangent $tg\delta$ (b).

$\Delta S_2 = 22.7 \pm 1.6 \text{ J}/(\text{mol K})$ ($\sim \ln 16$). The very large ΔS_2 value is the result of large atomic displacements in the reconstructive transformation.

The measurements of dielectric properties were carried out using an E7-20 immittance metre at a frequency of 1 kHz, upon heating and cooling at a rate of about 1.0 K/min in the temperature range 150–350 K. Since the crystals of $(\text{NH}_4)_3\text{TiF}_7$ were found to be cracked in the cooling–heating cycling [10], the study of ε and $tg\delta$ was performed on the “quasi-ceramic” sample in the form of a pressed pellet 8 mm in diameter and 1.05 mm in height. Copper electrodes were deposited on a sample in a vacuum.

In Fig. 3a and b, one can see the temperature dependencies of the permittivity and tangent of the dielectric losses. The dielectric constant shows the most pronounced anomalous behaviour near 290 K (Fig. 3c) associated with the increase from 8 up to 12 in the narrow temperature range and small change in the slope near 355 K. Vice versa, $tg\delta$ exhibits the abrupt step-wise change at about 360 K and change in the slope at 295 K. These temperatures are in good agreement with the phase transition temperatures found in experiments with an adiabatic calorimeter. A rather strong ε increase above 270 K is, most likely, connected with dielectric losses in the “quasi-ceramic” sample prepared without heat treatment.

Negligible anomalies in $\varepsilon(T)$ observed at T_1 and T_2 prove that phase transitions considered are not ferroelectric ones which are usually characterized by large values of permittivity (10^3 – 10^5) at phase transition point. These results agree well with the observation of the elastic domain structure in the G1 and G2 phases characteristic for ferroelastic transformations [10].

The temperature–pressure phase diagram of $(\text{NH}_4)_3\text{TiF}_7$ was studied using a DTA installation with a highly sensitive germanium–copper thermocouple to detect temperature associated with heat capacity anomalies. A powdered sample $5 \times 10^{-2} \text{ cm}^3$ in volume was placed in a small copper container glued onto one of two junctions of the thermocouple. A quartz sample as a reference substance was cemented to the other junction. After mounting, the system was then placed inside the piston-and-cylinder type vessel associated with the multiplier. Silicon oil was used as the pressure-transmitting medium to generate pressure up to 0.6 GPa. The measurements of temperature and pressure were performed with a copper–constantan thermocouple and manganin gauge with accuracies of about $\pm 0.3 \text{ K}$, and $\pm 10^{-3} \text{ GPa}$, respectively.

Fig. 4 shows the effect of hydrostatic pressure on the stability of the crystal phases in $(\text{NH}_4)_3\text{TiF}_7$. At ambient pressure two anomalies in the DTA-signal were recorded (Fig. 4a) associated with successive G1–G2–G3 phase transitions detected in optical DSC studies [10] as well as by adiabatic and dielectric measurements in the present paper. The reliability of the data obtained is supported by the reproducibility of the position of the phase boundaries in the phase diagram under increasing and decreasing pressures.

As the pressure increases, the temperatures T_1 and T_2 decrease and increase linearly, respectively, with the baric coefficients $dT_1/dp = -42 \text{ K/GPa}$ and $dT_2/dp = 18 \text{ K/GPa}$ (Fig. 4b). At $p \approx 0.12 \text{ GPa}$, the slope of the phase boundary between the G1 and G2 phases abruptly changes, with a strong decrease of $dT/dp = -164 \text{ K/GPa}$. Such a behaviour of the phase boundary allows us to suppose the

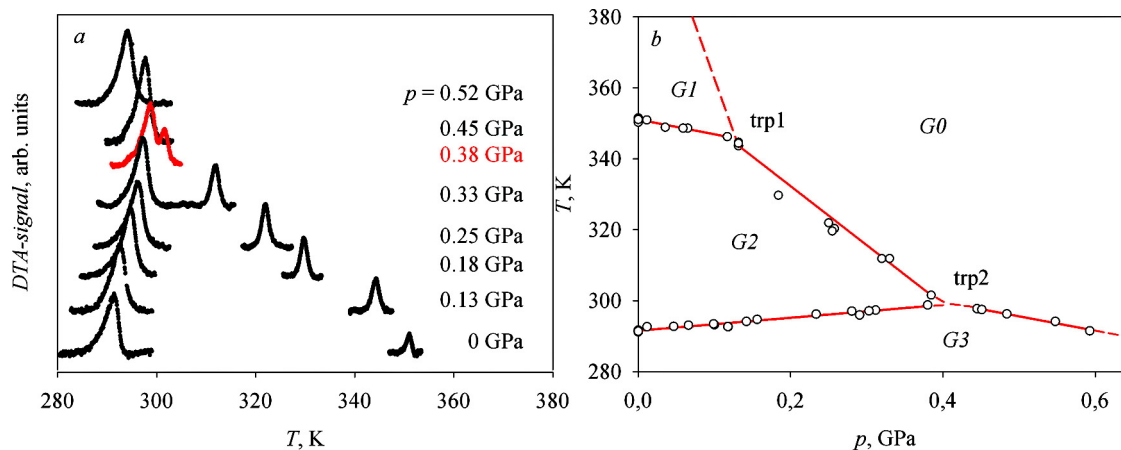


Fig. 4. Temperature dependencies of the DTA-signal at pressures in the range from 0 to 0.52 GPa (a), T–p phase diagram (b). Dashed line is the boundary between the G0 and G1 phases.

existence of a triple-point on the T–p phase diagram with parameters $T_{\text{trp1}} = 345.5$ K and $p_{\text{trp1}} = 0.125$ GPa.

And what about the third boundary at triple point 1? Analysis of complex twinning pictures in tetragonal phases G1 and G2 has allowed the existence of a high temperature cubic parent phase with $m\bar{3}m$ symmetry in $(\text{NH}_4)_3\text{TiF}_7$ to be assumed [10]. This hypothesis is corroborated by the cubic symmetry with the $Pm\bar{3}m$ ($Z = 1$) space group found at room temperature in some other double salt crystals with the formula A_3MeX_7 : $(\text{NH}_4)_3\text{SnF}_7$ [7] and $(\text{NH}_4)_3\text{PbF}_7$ [8]. Taking the results of [7,8,10] into account, one can reason that the third boundary at triple point 1 divides phases G1 and $G0 \equiv Pm\bar{3}m$.

The baric coefficient for the temperature of the $G0 \rightarrow G1$ phase transition can be evaluated considering the relation between entropy as well as volume changes around the triple-point.

The DTA technique is mainly able to register the entropy change in the temperature region close to phase transition point. Thus, the squares under DTA-signal peaks at $p = 0$ in Fig. 4a are associated with the entropy jumps $\delta S_{G1 \rightarrow G2}$ and $\delta S_{G2 \rightarrow G3}$. At $p > p_{\text{trp1}}$, the entropy is 1.5 times larger than $\delta S_{G1 \rightarrow G2}$. Thus, the $\delta S_{G0 \rightarrow G2}$ value can be considered as the sum of the $\delta S_{G0 \rightarrow G1}$ and $\delta S_{G1 \rightarrow G2}$ entropy changes. In accordance with the behaviour of excess entropy (Fig. 2), the entropy jumps at T_1 and T_2 are characterized by the values $\delta S_{G1 \rightarrow G2} = 2.9$ J/mol K and $\delta S_{G2 \rightarrow G3} = 12.9$ J/mol K, respectively. In such a case, the value of $\delta S_{G0 \rightarrow G2} \approx 1.5 \cdot \delta S_{G1 \rightarrow G2}$ is about 4.4 J/mol K and $\delta S_{G0 \rightarrow G1} \approx 1.5$ J/mol K. The relation between volume jumps around the triple-point is analogous: $\delta V_{G0 \rightarrow G2} = \delta V_{G0 \rightarrow G1} + \delta V_{G1 \rightarrow G2}$. Using experimental data on baric coefficients and entropy jumps, we evaluated the δV_i values around the triple-point 1 in the framework of Clapeyron–Clausius equation $dT/dp = \delta V/\delta S$; then the value of $dT_0/dp \equiv dT_{G0 \rightarrow G1}/dp$ was evaluated as equal to -600 K/GPa. This means that at ambient pressure the $G0 \rightarrow G1$ phase transition can take place at about 430 K. Such a huge negative baric coefficient as well as rather low temperatures of $(\text{NH}_4)_3\text{TiF}_7$ decomposition [10] and upper limit measurements on DTA installation (~ 360 K) are the reasons that the $G0 \rightarrow G1$ transformation was not detected in the present study at ambient and high pressure as well as in Ref. [10].

The second triple point was found with parameters $T_{\text{trp2}} = 298$ K and $p_{\text{trp2}} = 0.41$ GPa (Fig. 4b). Above p_{trp2} a direct phase transition between two cubic phases G0 and G3 takes place with a phase boundary characterized by a negative baric coefficient $dT_{G0 \rightarrow G3}/dp = -40$ K/GPa. The entropy jump at this transformation was evaluated comparing the squares of the DTA peaks associated, first, with the $G0 \rightarrow G2$ and $G0 \rightarrow G3$ phase transitions and, second, the $G1 \rightarrow G2$ and $G0 \rightarrow G3$ transitions. Both variants of the calculations gave almost the same result: $\delta S_{G0 \rightarrow G3} \approx 17.3$ J/mol K.

In accordance with T–p phase diagram (Fig. 4b), both G1 and G2 tetragonal phases are rather unstable in relation to pressure increase. Such a dramatic temperature change with pressure, which is characteristic for the transformation $G1 \rightarrow G0$, is a rarity and we do not know any similar example among compounds with the octahedral anions. However, some oxides with tetrahedral anions exhibit even more significant absolute values of baric coefficient: NH_4HSO_4 $dT/dp = 750$ K/GPa [14], Li_2WO_4 $dT/dp = 1200$ K/GPa [15]. High susceptibility to pressure is one the most important properties of materials which are considered as solid state refrigerants operated on the ground of barocaloric effect [16].

In the present paper and [10], we have found and studied phase transitions in titanium fluoride $(\text{NH}_4)_2\text{TiF}_6 \cdot \text{NH}_4\text{F}$ with the isolated octahedral species TiF_6^{2-} . There exist a lot of fluoride compounds containing $[\text{Ti}_x\text{F}_{4x+y}]^y$ anions with the vertex-sharing octahedral TiF_6 units, partially studied in [17], which also can be considered

as the promising systems to undergo structural transformations. Such a supposition is confirmed by the results of structural studies of some compounds containing $[\text{Ti}_4\text{F}_{20}]^{4-}$ and $[\text{Ti}_2\text{F}_9]^-$ anions at room temperature and 200 K [17].

3. Conclusions

Detailed studies of heat capacity, dielectric properties and susceptibility to hydrostatic pressure at the unusual sequence of phase transitions in the fluoride double salt $(\text{NH}_4)_3\text{TiF}_7$ have been performed.

Rather large entropies of phase transitions $G1 \rightarrow G2$ and $G2 \rightarrow G3$ were found, consisting of comparable values of the δS jumps at phase transition points and contributions $\Delta S(T)$ associated with the temperature dependence of the excess heat capacity over rather wide temperature ranges.

The nonferroelectric nature of both transformations was confirmed by the behaviour of the permittivity and dielectric loss tangent.

The study of the temperature–pressure phase diagram revealed two triple-points and the existence of the hypothetical parent $G0 \equiv Pm\bar{3}m$ cubic phase lying at ambient pressure above the decomposition temperature of $(\text{NH}_4)_3\text{TiF}_7$.

Depending on the symmetry of the low temperature phase in relation to $G0 \equiv Pm\bar{3}m$, the phase boundaries are characterized by rather different baric coefficients: $dT_{G0 \rightarrow G1}/dp = -600$ K/GPa, $dT_{G0 \rightarrow G2}/dp = -164$ K/GPa, $dT_{G0 \rightarrow G3}/dp = -40$ K/GPa. $(\text{NH}_4)_3\text{TiF}_7$ undergoes a transformation between two cubic phases $G0 \rightarrow G3$ near room temperature and $p > 0.41$ GPa.

Acknowledgements

This work was supported by the Russian Foundation for Basic Research (Grant no. 15-02-02009), and the Council on Grants from the President of the Russian Federation for the Support of Leading Scientific Schools of the Russian Federation (Grant no. NSh-924.2014.2).

References

- [1] K.S. Aleksandrov, A.T. Anistratov, B.V. Beznosikov, N.V. Fedoseeva, Phase Transitions in Crystals of ABX₃ Halides, Nauka, Novosibirsk, 1981 (in Russian).
- [2] K.S. Aleksandrov, B.V. Beznosikov, Perovskite-like Crystals, Novosibirsk, Nauka, 1997 (in Russian).
- [3] I.N. Flerov, M.V. Gorev, K.S. Aleksandrov, A. Tressaud, J. Grannec, M. Couzi, Mater. Sci. Eng. R24 (1998) 81–150.
- [4] D.L. Deadmore, W.F. Bradley, Acta Crystallogr. 15 (1962) 186–189.
- [5] J.L. Hoard, M.B. Williams, J. Am. Soc. 64 (1942) 633–637.
- [6] C. Plitzko, G. Meyer, Z. Kristallogr. NCS 213 (1998) 475.
- [7] C. Plitzko, G. Meyer, Z. Anorg. Allg. Chem. 623 (1997) 1347–1348.
- [8] U. Reusch, E. Schweda, Mater. Sci. Forum 378–381 (2001) 326–330.
- [9] A. Vasiliev, N. Laptash, Inst. of Physics Krasnoyarsk, Russia, ICDD Grant-in-Aid, 2003.
- [10] S.V. Mel'nikova, E.I. Pogoreltsev, I.N. Flerov, N.M. Laptash, J. Fluorine Chem. 165 (2014) 14–19.
- [11] A.V. Kartashev, I.N. Flerov, N.V. Volkov, K.A. Sablina, Phys. Solid State 50 (2008) 2115–2120.
- [12] V.D. Fokina, E.V. Bogdanov, M.V. Gorev, M.S. Molokeev, E.I. Pogoreltsev, I.N. Flerov, N.M. Laptash, Phys. Solid State 52 (2010) 781–788.
- [13] V.D. Fokina, I.N. Flerov, A.F. Bovina, M.V. Gorev, N.M. Laptash, E.V. Bogdanov, Phys. Solid State 49 (2007) 1548–1553.
- [14] I.N. Polandov, V.P. Mylov, B.A. Strukov, Fizika Tverdogo Tela 10 (1968) 2232–2234 (in Russian).
- [15] C.W.F.T. Pistorius, J. Solid State Chem. 13 (1975) 325–329.
- [16] I.N. Flerov, M.V. Gorev, A. Tressaud, N.M. Laptash, Crystallogr. Rep. 56 (2011) 9–17.
- [17] I.M. Shlyapnikov, H.P.A. Mercier, E.A. Goreschnik, G.J. Schrobilgen, Z. Mazej, Inorg. Chem. 52 (2013) 8315–8326.